ACS Sustainable Chemistry & Engineering

pubs.acs.org/journal/ascecg

Letter

Interface Engineering of CoS_2−CeO_2/Ti Nanocatalyst for Artificial N_2 Fixation

Jinzhi Zhou, Xuejing Liu, Xiaolong Xu, Xu Sun, Dan Wu, Hongmin Ma, Xiang Ren,* Qin Wei,* and Huangxian Ju*

Cite This: *ACS Sustainable Chem. Eng.* 2021, 9, 13399−13405

Read Online

ACCESS | Metrics & More | Article Recommendations | Supporting Information

ABSTRACT: The development of a highly selective electrocatalytic nitrogen reduction ammonia catalyst is an attractive and challenging task. In this letter, we reported the construction of a CoS_2−CeO_2 load on Ti mesh (CoS_2−CeO_2/Ti) based on interface engineering, which can be used as a highly efficient electrocatalytic nitrogen reduction reaction (NRR) catalyst under environmental conditions. According to density functional theory (DFT) calculations, N_2 can be activated by the low-coordinated Co atom of the CoS_2(110) surface, and the construction of a CoS_2/CeO_2 interface can effectively provide the necessary H^+ for NRR, realizing the improvement of catalytic activity. In 0.1 M Na_2SO_4, CoS_2−CeO_2/Ti achieved a considerable average NH_3 yield rate of 3.33×10^{-10} mol s^{-1} cm^{-2} and Faraday efficiency (FE) of 2.52% at −0.5 V vs RHE. Therefore, its performance is better than that of many known NRR electrocatalysts.

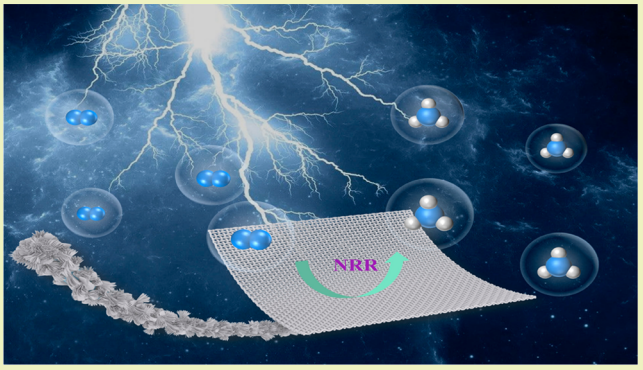

KEYWORDS: *Electrocatalysis, N_2 reduction reaction, Interface engineering, Selective vulcanization, CoS_2−CeO_2/Ti, Density functional theory*

INTRODUCTION

As an important chemical and fertilizer raw material, NH_3 plays an irreplaceable role in industry and agriculture. At the same time, regarding NH_3 as a new energy carrier, the weight ratio of hydrogen in liquid NH_3 was 17.6% and that in methanol was 12.5%.[1,2] In the future, NH_3 will be very promising in terms of the hydrogen economy and a significant part of the development of new energy materials.[3,4] Today, with the increasing demand for NH_3, people have made more in-depth research on the large-scale artificial production technology of NH_3. It is very difficult to synthesize NH_3 under mild conditions because nitrogen molecules are inert, and N≡N bond splitting requires a large energy barrier. However, the commonly used Haber−Bosch method must be carried out at 350−550 °C and 150−350 atmospheres,[5−7] leading excessive emission of carbon dioxide,[8,9] which has seriously violated the concept of sustainable development. Therefore, the exploration of a clean, efficient, and sustainable NH_3 production method remains a huge challenge. Several strategies for NH_3 synthesis by artificial nitrogen fixation have been developed, including electrocatalysis, photocatalysis, and biological strategies.[10−18] The electrocatalytic nitrogen reduction reaction (NRR) for NH_3 production stands out among many NH_3 production methods due to its advantages of having a mild, safe, controllable, and simple process.

Because of the huge adsorption barrier of nitrogen molecules, a strong dipole moment, and interference produced by the electrocatalytic hydrogen evolution reaction (HER),[19,20] it requires a highly selective, active, and efficient electrocatalyst. Precious metals are effective catalysts for NRR,[21,22] but their scarcity and high cost prevent them from being widely used. The unique d-orbital structures of transition metals and electron donors with rich electron cloud densities are beneficial to weaken the stable N≡N bond and realize efficient N_2 activation.[23,24] Recently, studies have shown that Co single-atom clusters have a good catalytic effect on NRR.[25] The S element is an essential component in nitrogenase. CoS_2 may exhibit good NRR performance, and S can regulate the electronic properties of Co and the adsorption energy of intermediates.[26] In order to balance nitrogen activation and hydrogen evolution, interface engineering plays an important role.[27,28] The controllable interface effect can form a bridge key, which provides electron transfer channels and accelerates

Received: September 10, 2021
Revised: September 24, 2021
Published: September 28, 2021

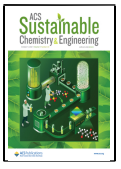

the electron transfer rate.[29] Metal/(hydroxide) oxide interface engineering can effectively improve the performance of metal catalysts.[30] It is reported that the rare earth oxide CeO_2-supported metal has good catalytic activity for NRR.[31−36] The interface between the transition metal compound and CeO_2 can provide H^+ for NRR;[37] thus, the combination of CeO_2 to CoS_2 can effectively promote NRR efficiency. In addition, theoretical calculations also show that CeO_2 is very important for improving the performance of NRR.[38] On the basis of the above factors, we raise a strategy about selective vulcanization, an effective CoS_2−CeO_2 nanocatalyst constructed from the precursor of Co_3O_4−CeO_2 hybrids, only to convert Co_3O_4 to CoS_2 and CeO_2 to keep it unchanged.

The as-synthesized CoS_2−CeO_2/Ti nanopcatalyst prepared on Ti mesh can effectively convert N_2 into NH_3 under mild conditions. In 0.1 M Na_2SO_4, the NH_3 yield rate is 3.33×10^{-10} mol s^{-1} cm^{-2}, and FE is 2.52% at −0.5 V vs RHE, which are significantly higher than those of the Co_3O_4−CeO_2/Ti precursor (NH_3 yield rate is 1.06×10^{-10} mol s^{-1} cm^{-2}, FE is 1.01%) and most known NRR electrocatalysts. Surprisingly, the catalyst also has outstanding selectivity and electrochemical perdurability.

RESULTS AND DISCUSSION

The X-ray diffraction (XRD) pattern of Co_3O_4−CeO_2 is presented in Figure 1a, which can clearly correspond to Co_3O_4 (JCPDS No. 43-1003) and CeO_2 (JCPDS No. 34-0394). Interestingly, CoS_2−CeO_2/Ti was prepared successfully by selective sulfuration, and its XRD is displayed in Figure 1b. It

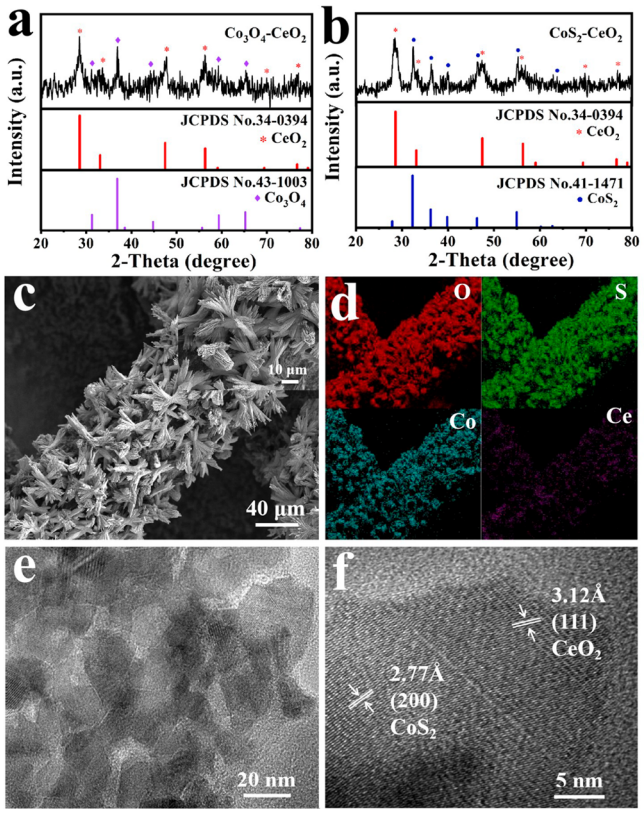

Figure 1. (a) XRD pattern of (a) Co_3O_4−CeO_2/Ti and (b) CoS_2−CeO_2/Ti. (c) SEM image of CoS_2−CeO_2/Ti. (d) EDX mapping of O, S, Co, and Ce for CoS_2−CeO_2/Ti. (e) TEM and (f) HRTEM image of CoS_2−CeO_2/Ti.

can be seen in the figure that the five typical peaks near 32.3°, 36.2°, 39.8°, 46.3°, and 54.9° correspond to (200), (210), (211), (220), and (311) diffraction surfaces of CoS_2 (JCPDS No. 41-1471). The other four typical peaks around 28.6°, 33.1°, 47.5°, and 56.3° correspond to the (111), (200), (220), and (311) of CeO_2 planes (JCPDS No. 34-0394), respectively. It is shown (SEM, Figure 1c) that the surface of the Ti mesh was completely covered, and the morphology of CoS_2−CeO_2/Ti was a nanosheet. In the energy dispersive X-ray (EDX) element diagram (Figure 1d), it can be further shown that the Co, Ce, S, and O elements in CoS_2−CeO_2/Ti are uniformly distributed, and the atomic ratio of Co:S:Ce:O is 8.34:18.14:5.24:68.27 (Figure S1). A high-resolution TEM (HRTEM) image (Figure 1f) was obtained for the CoS_2−CeO_2 nanosheet (Figure 1e), showing that there are 2.77 and 3.12 Å lattice fringes on CoS_2 (200) and CeO_2 (111), respectively.

The characteristic peaks of the X-ray photoelectron spectroscopy (XPS) of Co, S, Ce, and O are presented in Figure 2a−d, and the total XPS measurement spectrum of

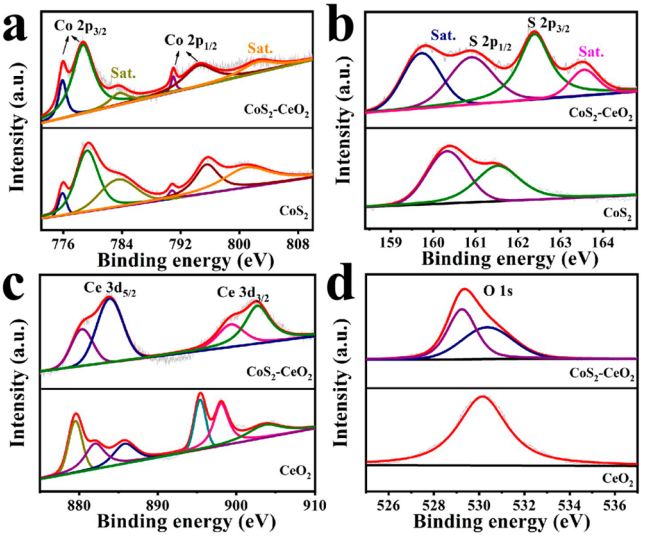

Figure 2. XPS spectra of CoS_2−CeO_2/Ti nanocatalyst in (a) Co 2p, (b) S 2p, (c) Ce 3d, and (d) O 1s regions.

CoS_2−CeO_2/Ti is presented in Figure S2. According to the Co 2P spectra (Figure 2a), the Co $2p_{3/2}$ region corresponds to two binding energy peaks of 775.9 and 778.7 eV. There is also an oscillating satellite peak. The Co $2p_{1/2}$ region corresponds to two binding energy peaks of 790.8 and 795.1 eV. There is also another oscillating satellite peak.[39,40] In the S 2p region (Figure 2b), S $2p_{1/2}$ and S $2p_{3/2}$ correspond to two binding energy peaks of 161.09 and 162.59 eV, respectively. It is noteworthy that, compared with pure CoS_2, the peaks in both the Co 2p region and S 2p region have a positive shift, which is considered to be the effect of interface formation. In the Ce 3d region (Figure 2c), Ce $3d_{5/2}$ corresponds to two binding energy peaks at 880.36 and 883.9 eV. Binding energy peaks at 899.31 and 902.68 eV are assigned to Ce $3d_{3/2}$, which are related to Ce^{4+} and Ce^{3+} in CeO_2, respectively. Compared with pure CeO_2, the peak of the Ce 3d region also shifted positively. Figure 2d shows the XPS spectra of the O 1s region, and the two binding energy peaks at 529.24 and 530.36 eV can be ascribed to O^{2-} enhancement in NRR catalysis. These surveys indicate that the electronic interaction between CoS_2 and

https://doi.org/10.1021/acssuschemeng.1c05850
ACS Sustainable Chem. Eng. 2021, 9, 13399−13405

CeO_2 in CoS_2−CeO_2 likely provide help in enhancing the catalytic effect of NRR.

Electrocatalytic NRR is an experiment conducted in an H-type electrolytic cell under environmental conditions and separated by a Nafion 115 membrane. The Nafion 115 membrane allows the penetration of H^+ and restricts the diffusion of NH_3, thereby effectively avoiding the oxidation of NH_3. This experiment used a traditional three-electrode system, the Na_2SO_4 electrolyte was annealed at high temperature before use in order to eliminate the interference of nitrate and nitrite. All experiments were conducted under environmental conditions.

The linear sweep voltammetry (LSV) curve of CoS_2−CeO_2/Ti is displayed in Figure 3a, and the polarization curve (red line) obtained when N_2 was applied has a higher current density, which is due to the NRR reaction of CoS_2−CeO_2/Ti. In addition, the LSV curve determined the NRR performance from −0.3 to −0.7 V (vs RHE), and current density curves plotted at different potentials change with time, as shown in Figure 3b. The indophenol blue method was used to analyze the obtained NH_3, and the Watt and Chrisp[41] method was used to determine the possible byproduct (N_2H_4) (the Supporting Information contains specific steps). The required test calibration curves (Figures S3 and S4) show a good linear relationship. The UV−vis absorption spectra of the bath solution at each potential after 1 h of a chromogenic reaction are shown in Figure 3c, indicating a significant catalytic effect. Figure 3d displays the best potential at −0.5 V, and the average NH_3 yield rate is 3.33×10^{-10} mol s^{-1} cm^{-2} with FE of 2.52%. The catalyst outperformed many known NRR catalysts, including Mo nanofilm (3.09×10^{-11} mol s^{-1} cm^{-2}) and Fe_3O_4/Ti (5.6×10^{-11} mol s^{-1} cm^{-2}). There also exist some reported catalysts with much better NRR performances, like the Fe, Mo−N/C catalyst (1.52×10^{-6} mol h^{-1} cm^{-2}, 14.2%).[42] Table S1 lists more comparative information on NRR electrocatalyst activity under environmental conditions. Figure S5 indicates that CoS_2−CeO_2/Ti did not generate N_2H_4 during the catalytic process, thus showing excellent selectivity. The low FE of the NRR catalysis process may be due to the side reaction of hydrogen evolution and the capacitance of the Ti support as well as dynamic hydrogen adsorption and absorption on the catalyst.[5,19,43]

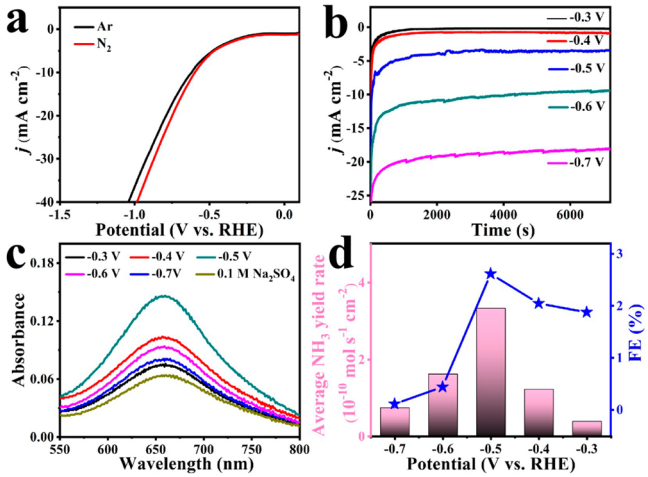

Figure 3. (a) LSV curves of the NRR test of CoS_2−CeO_2/Ti in Ar and N_2 saturated electrolytes. (b) Curve of current density with time of CoS_2−CeO_2/Ti under selected potential interval. (c) UV−vis absorption spectra of CoS_2−CeO_2/Ti under selected potentials. (d) Average NH_3 yield rate and FE of CoS_2−CeO_2/Ti under specified potentials.

Several sets of control experiments were designed to prove the preparation of NH_3 by CoS_2−CeO_2/Ti electrocatalytic NRR for convenience. The curves of the current densities with time of Ti, CoS_2/Ti, Co_3O_4−CeO_2 /Ti, and CoS_2−CeO_2/Ti at −0.5 V are displayed in Figure 4a. Through the analysis of Figure 4b, it is found that the pure Ti mesh has almost no catalytic performance. Compared with CoS_2/Ti, CoS_2−CeO_2/Ti has more excellent catalytic activity, which can prove that the strategy of using CeO_2 to form the interface can accelerate the electron transfer rate and improve catalytic performance. Compared with Co_3O_4−CeO_2/Ti, the catalytic performance of CoS_2−CeO_2/Ti is significantly improved, indicating that selective vulcanization has a significant effect on NRR, which is attributed to the fact that S doping can effectively adjust the electronic structure and provide active sites to improve catalytic performance.[25] In order to further study the phenomenon of charge transfer on the reaction interface of the catalyst, an electrochemical impedance spectroscopy (EIS) test was carried out on CoS_2, CeO_2, and CoS_2−CeO_2 (Figure S6). The results verify that CoS_2−CeO_2 has a smaller impedance value and therefore a higher charge transfer rate, which again confirms its high NRR performance. Next, four sets of comparative experiments are carried out at the same time (Figure 4c). The UV−vis absorption spectra of the electrolyte solution under disparate electrochemical conditions is shown in Figure S7. Surprisingly, there is no NH_3 generated

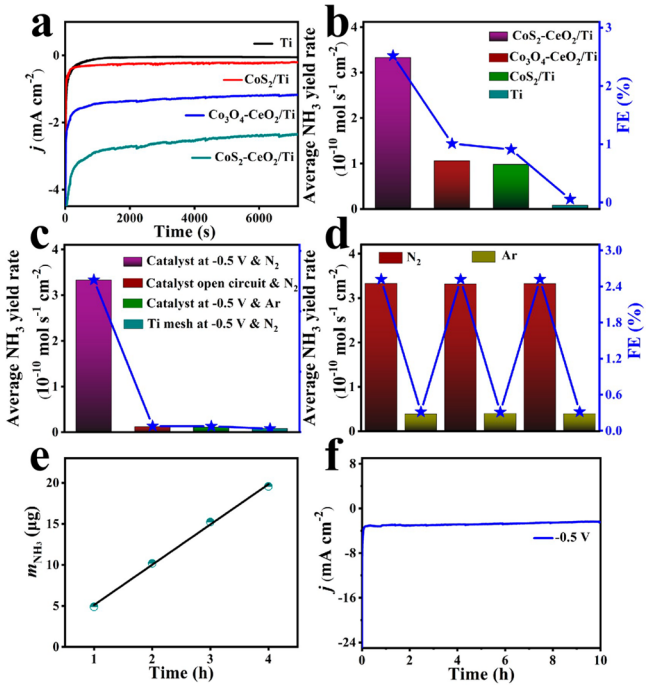

Figure 4. (a) Curve of current density with time and (b) average NH_3 yield rate and FE of Ti, CoS_2/Ti, Co_3O_4−CeO_2/Ti, and CoS_2−CeO_2/Ti at −0.5 V. (c) Average NH_3 yield rate and FE of the four groups of comparative experiments. (d) Average NH_3 yield rate and FE alternately tested 2 h of CoS_2−CeO_2/Ti in N_2- and Ar-saturated electrolytes at −0.5 V. (e) Linear curve of m_{NH3} vs reaction time at −0.5 V. (f) Curve of current density with time for 10 h.

https://doi.org/10.1021/acssuschemeng.1c05850
ACS Sustainable Chem. Eng. 2021, 9, 13399−13405

in the comparative experiments (1), (2), and (3). The results in Figure 4b show that NH_3 can only be produced in N_2-saturated electrolytes. In addition, m_{NH3} and reaction time have a linear relationship (Figure 4e). At the same time, $^{15}N_2$ isotope labeling experiments have been carried out (Figure S8). When $^{15}N_2$ is used as the raw gas, the double coupling corresponds to $^{15}NH_4^+$ appearing in the ^1H nuclear magnetic resonance (NMR) spectrum, which is $^{15}NH_4Cl$ in accordance with the standard ^1H NMR spectrum, indicating that the N element of the NH_3 product comes from providing N_2. There is no doubt that the above evidence proves that NH_3 is produced by the electrocatalytic NRR of CoS_2−CeO_2/Ti.

Stability and reproducibility are important foundations for measuring the performance of catalysts.[44,45] The curve of current density with time of CoS_2−CeO_2/Ti after 10 h of continuous catalysis is represented in Figure 4f, which has almost no fluctuation. After NRR electrolysis for 10 h compared to 2 h, both NH_3 yield rate and FE only decreased negligibly (Figure S9). It shows that after a long-term catalytic test, CoS_2−CeO_2/Ti still has excellent performance for catalytic reduction of N_2 to NH_3. Meanwhile, the morphology with the nanocatalyst remained the same shape after long-term electrolysis. The SEM and TEM characterizations after electrolysis are shown in Figures S10 and S11, further demonstrating the stability and durability. Figure S12 shows that CoS_2−CeO_2/Ti has no significant change in NH_3 yield rate and FE in 6 cycles, indicating that CoS_2−CeO_2/Ti has excellent NRR reproducibility. We finally tested the influence of different N_2 flow rates for NRR experiments (Figure S13). From the experimental results, the conclusion that the N_2 diffusion rate is not the decision step can be drawn.

The NRR mechanism on the CoS_2−CeO_2 interface and CoS_2 surfaces is further illustrated using DFT calculations. According to the XRD and HRTEM results (JCPDS No. 41-1471), we constructed the CoS_2−CeO_2 interface and the (110) and (100) surfaces of the CoS_2 as described in the Supporting Information). We first studied the NRR mechanism and intermediate structures on different CoS_2 surfaces (Figure S14 and inset). The results show that the N_2 molecule is physically adsorbed on the CoS_2(100) surface, while the N_2 molecule can be activated by the low-coordination Co atom of the CoS_2(110) surface, and the N≡N bond length of adsorbed N_2 (1.129 Å) is longer than that of free nitrogen (1.098 Å). The hydrogenation process from $*N_2$ to *NNH on the CoS_2(110) surface consumes 1.05 eV of free energy (ΔG), which is the potential-determining step (PDS). After that, the hydrogenation of *NNH involves two pathways of distal and alternative hydrogenations. In order to illustrate the role of CeO_2, we further studied the adsorption of N_2 and H_2O molecules and the ΔG of the NRR process on the CoS_2−CeO_2 interface containing oxygen vacancies based on the experimental characterization (Figure 5). The results show that the adsorption of H_2O on the surface of CeO_2 containing an oxygen vacancy is stronger than that of the physically adsorbed N_2. Therefore, we studied the NRR process at the CoS_2−CeO_2 interface with H_2O adsorption. The results show that the N≡N bond length of the adsorbed N_2 (1.132 Å) is longer than that of the above CoS_2(110) surfaces, which confirms that the CoS_2−CeO_2 interface with adsorbed H_2O molecules enhances the activation of N_2. Also, the differential charge density further shows the charge distribution of the adsorbed H_2O and N_2 molecules (Figure 5a). In addition, according to Bader charge analysis, about 0.16e electrons are transferred from

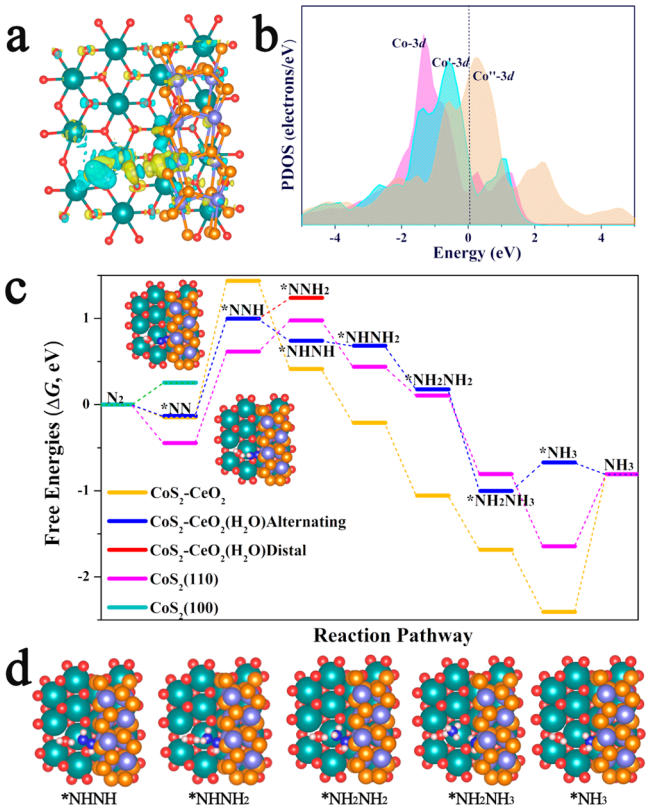

Figure 5. (a) Different charge densities of H_2O and N_2 adsorptions on the CoS_2−CeO_2 interface (isosurface value of 0.0021 e/bohr^3). (b) Partial density of states (PDOS) of the Co-3d, Co′-3d and Co″-3d states in the CoS_2−CeO_2 with N_2 adsorption and CoS_2−CeO_2 and CoS_2 systems, respectively. (c) Calculated free energy diagram of NRR on different CoS_2 surfaces and CoS_2−CeO_2 interface. (d) Optimized intermediates during the NRR process on the CoS_2−CeO_2 interface with H_2O molecules. Co, Ce, S, O, N, and H atoms are represented by light blue, green, orange, red, royal blue, and pink balls, respectively.

CoS_2 to CeO_2, and the density of states (PDOS) diagram shows that the PDOS of the Co-3d state at the CoS_2−CeO_2 interface shifts to the left (Figure 5b), suggesting that they are advantageous to activate N_2 molecules. Then, the ΔG values of the NRR process on the CoS_2−CeO_2 interface and CoS_2 surfaces were compared, as shown in Figure 5c, and the intermediate structures are displayed in Figure 5d. For the first hydrogenation from $*N_2$ to *NNH as PDS, the ΔG of this uphill pathway is 1.12 eV, which is comparable to the energy barrier of PDS on the CoS_2(110) surface. It is worth noting that the adsorbed H_2O can greatly reduce the energy barrier of the first hydrogenation to form *NNH species, indicating that it can decrease the overpotential to enhance the electrocatalytic activity of NRR. After that, the energy consumed by the alternative hydrogenation pathway from *NNH to *NHNH is −0.25 eV, which is smaller than that from *NNH to $*NNH_2$ species (0.24 eV). The subsequent three hydrogenation steps from *NHNH species is a downhill pathway, while it can be seen that the desorption of NH_3 is more favorable than other surfaces. Overall, we conclude that the increment of NRR activity mainly originates from the low-coordinated Co sites on the CoS_2(110) and CoS_2−CeO_2 interface, and the H_2O adsorption on the CeO_2 containing oxygen vacancies can significantly reduce the overpotential of NRR.

https://doi.org/10.1021/acssuschemeng.1c05850
ACS Sustainable Chem. Eng. 2021, 9, 13399−13405

CONCLUSION

In conclusion, the CoS_2−CeO_2/Ti nanocatalyst proved to be an effective selective electrocatalyst for NRR under environmental conditions. The average NH_3 yield rate of CoS_2−CeO_2/Ti is 3.33×10^{-10} mol s^{-1} cm^{-2} with FE of 2.52% at −0.5 V (vs RHE). At the same time, high selectivity and good electrochemical durability have also been demonstrated. This study provides a new direction for the research and development of high-efficiency NRR catalysts prepared by interface engineering.

ASSOCIATED CONTENT

Supporting Information

The Supporting Information is available free of charge at https://pubs.acs.org/doi/10.1021/acssuschemeng.1c05850.

Experimental details, EDX elemental spectrum image of CoS_2−CeO_2/Ti, XPS survey spectrum for CoS_2−CeO_2/Ti, calibration curve for detecting the concentration of NH_3 and N_2H_4, UV−vis absorption spectra of electrolyte solution under different electrochemical conditions, average NH_3 yield rate and FE after charging at −0.5 V (vs RHE) for 2 and 10 h under ambient conditions, average NH_3 yield rate and FE at different N_2 flow rates at −0.5 V (vs RHE) on the CoS_2−CeO_2/Ti electrode, and more comparative information (Table S1) (PDF)

AUTHOR INFORMATION

Corresponding Authors

Xiang Ren − *Key Laboratory of Interfacial Reaction & Sensing Analysis in Universities of Shandong, School of Chemistry and Chemical Engineering, University of Jinan, Jinan 250022 Shandong, China; Collaborative Innovation Center for Green Chemical Manufacturing and Accurate Detection, Jinan 250022 Shandong, China;* orcid.org/0000-0002-4321-4282; Email: chem_renx@163.com

Qin Wei − *Key Laboratory of Interfacial Reaction & Sensing Analysis in Universities of Shandong, School of Chemistry and Chemical Engineering, University of Jinan, Jinan 250022 Shandong, China; Collaborative Innovation Center for Green Chemical Manufacturing and Accurate Detection, Jinan 250022 Shandong, China;* orcid.org/0000-0002-3034-8046; Email: sdjndxwq@163.com

Huangxian Ju − *Key Laboratory of Interfacial Reaction & Sensing Analysis in Universities of Shandong, School of Chemistry and Chemical Engineering, University of Jinan, Jinan 250022 Shandong, China; State Key Laboratory of Analytical Chemistry for Life Science, College of Chemistry and Chemical Engineering, Nanjing University, Nanjing 210023, P. R. China;* orcid.org/0000-0002-6741-5302; Email: hxju@nju.edu.cn

Authors

Jinzhi Zhou − *Key Laboratory of Interfacial Reaction & Sensing Analysis in Universities of Shandong, School of Chemistry and Chemical Engineering, University of Jinan, Jinan 250022 Shandong, China*

Xuejing Liu − *Key Laboratory of Interfacial Reaction & Sensing Analysis in Universities of Shandong, School of Chemistry and Chemical Engineering, University of Jinan, Jinan 250022 Shandong, China;* orcid.org/0000-0003-3644-0369

Xiaolong Xu − *Key Laboratory of Interfacial Reaction & Sensing Analysis in Universities of Shandong, School of Chemistry and Chemical Engineering, University of Jinan, Jinan 250022 Shandong, China*

Xu Sun − *Key Laboratory of Interfacial Reaction & Sensing Analysis in Universities of Shandong, School of Chemistry and Chemical Engineering, University of Jinan, Jinan 250022 Shandong, China;* orcid.org/0000-0001-8762-4243

Dan Wu − *Key Laboratory of Interfacial Reaction & Sensing Analysis in Universities of Shandong, School of Chemistry and Chemical Engineering, University of Jinan, Jinan 250022 Shandong, China; Collaborative Innovation Center for Green Chemical Manufacturing and Accurate Detection, Jinan 250022 Shandong, China;* orcid.org/0000-0002-8732-5988

Hongmin Ma − *Key Laboratory of Interfacial Reaction & Sensing Analysis in Universities of Shandong, School of Chemistry and Chemical Engineering, University of Jinan, Jinan 250022 Shandong, China; Collaborative Innovation Center for Green Chemical Manufacturing and Accurate Detection, Jinan 250022 Shandong, China;* orcid.org/0000-0002-7061-8944

Complete contact information is available at: https://pubs.acs.org/10.1021/acssuschemeng.1c05850

Notes

The authors declare no competing financial interest.

ACKNOWLEDGMENTS

This study was supported by the National Key Scientific Instrument and Equipment Development Project of China (No. 21627809), Natural Science Foundation of Shandong Province (No. 2019GSF111023), Jinan Scientific Research Leader Workshop Project (2018GXRC024), and Innovation Team Project of Colleges and Universities in Jinan (No. 2019GXRC027).

REFERENCES

(1) Wijayanta, A. T.; Oda, T.; Purnomo, C. W.; Kashiwagi, T.; Aziz, M. Liquid Hydrogen, Methylcyclohexane, and Ammonia as Potential Hydrogen Storage: Comparison review. *Int. J. Hydrogen Energy* **2019**, *44*, 15026−15044.

(2) Guo, J.; Chen, P. Catalyst: NH_3 as an Energy Carrier. *Chem.* **2017**, *3*, 709−712.

(3) Kojima, Y.; Yamaguchi, M. Ammonia Storage Materials for Nitrogen Recycling Hydrogen and Energy Carriers. *Int. J. Hydrogen Energy* **2020**, *45*, 10233−10246.

(4) Guo, W.; Zhang, K.; Liang, Z.; Zou, R.; Xu, Q. Electrochemical Nitrogen Fixation and Utilization: Theories, Advanced Catalyst Materials and System Design. *Chem. Soc. Rev.* **2019**, *48*, 5658−5716.

(5) Ren, X.; Zhao, J.; Wei, Q.; Ma, Y.; Guo, H.; Liu, Q.; Wang, Y.; Cui, G.; Asiri, A. M.; Li, B.; Tang, B.; Sun, X. High-Performance N_2-to-NH_3 Conversion Electrocatalyzed by Mo_2C Nanorod. *ACS Cent. Sci.* **2019**, *5*, 116−121.

(6) Chen, G.; Ren, S.; Zhang, L.; Cheng, H.; Luo, Y.; Zhu, K.; Ding, L.; Wang, H. Nitrogen Reduction Reactions: Advances in Electrocatalytic N_2 Reduction—Trategies to Tackle the Selectivity Challeng. *Small Methods* **2019**, *3*, 1970016.

(7) Mukherjee, S.; Cullen, D. A.; Karakalos, S.; Liu, K.; Zhang, H.; Zhao, S.; Xu, H.; More, K. L.; Wang, G.; Wu, G. Metal-Organic Framework-Derived Nitrogen-Doped Highly Disordered Carbon for Electrochemical Ammonia Synthesis Using N_2 and H_2O in alkaline electrolytes. *Nano Energy* **2018**, *48*, 217−226.

(8) Guo, C.; Ran, J.; Vasileff, A.; Qiao, S. Rational Design of Electrocatalysts and Photo(electro)catalysts for Nitrogen Reduction

to Ammonia (NH_3) under Ambient Conditions. *Energy Environ. Sci.* **2018**, *11*, 45−56.
(9) Wu, Q.; Gao, Q.; Sun, L.; Guo, H.; Tai, X.; Li, D.; Liu, L.; Ling, C.; Sun, X. Facilitating Active Species by Decorating CeO_2 on Ni_3S_2 Nanosheets for Efficient Water Oxidation Electrocatalysis. *Chin. J. Catal.* **2021**, *42*, 482−489.
(10) Li, P.; Zhang, T.; Mushtaq, M. A.; Wu, S.; Xiang, X.; Yan, D. Research Progress in Organic Synthesis by Means of Photoelectrocatalysis. *Chem. Rec.* **2021**, *21*, 841−857.
(11) Chen, G.; Yuan, Y.; Jiang, H.; Ren, S.; Ding, L.; Ma, L.; Wu, T.; Lu, J.; Wang, H. Electrochemical Reduction of Nitrate to Ammonia Via Direct Eight-electron Transfer Using a Copper-Molecular Solid Catalyst. *Nat. Energy* **2020**, *5*, 605−613.
(12) Xing, P.; Wu, S.; Chen, Y.; Chen, P.; Hu, X.; Lin, H.; Zhao, L.; He, Y. New Application and Excellent Performance of $Ag/KNbO_3$ Nanocomposite in Photocatalytic NH_3 Synthesis. *ACS Sustainable Chem. Eng.* **2019**, *7*, 12408−12418.
(13) Liao, Y.; Qian, J.; Xie, G.; Han, Q.; Dang, W.; Wang, Y.; Lv, L.; Zhao, S.; Luo, L.; Zhang, W.; Jiang, H.; Tang, J. 2D-layered Ti_3C_2 MXenes for Promoted Synthesis of NH_3 on P25 Photocatalysts. *Appl. Catal., B* **2020**, *273*, 119054.
(14) Liu, H.; Wu, P.; Li, H.; Chen, Z.; Wang, L.; Zeng, X.; Zhu, Y.; Jiang, Y.; Liao, X.; Haynes, B. S.; Ye, J.; Stampfl, C.; Huang, J. Unravelling the Effects of Layered Supports on Ru Nanoparticles for Enhancing N_2 Reduction in Photocatalytic Ammonia Synthesis. *Appl. Catal., B* **2019**, *259*, 118026.
(15) Zhu, X.; Mou, S.; Peng, Q.; Liu, Q.; Luo, Y.; Chen, G.; Gao, S.; Sun, X. Aqueous Electrocatalytic N_2 Reduction for Ambient NH_3 Synthesis: Recent Advances in Catalyst Development and Performance Improvement. *J. Mater. Chem. A* **2020**, *8*, 1545−1556.
(16) Zhao, S.; Lu, X.; Wang, L.; Gale, J.; Amal, R. Carbon-Based Metal-Free Catalysts for Electrocatalytic Reduction of Nitrogen for Synthesis of Ammonia at Ambient Conditions. *Adv. Mater.* **2019**, *31*, 1805367.
(17) Honkala, K.; Hellman, A.; Remediakis, I. N.; Logadottir, A.; Carlsson, A.; Dahl, S.; Christensen, C. H.; Nørskov, J. K. Ammonia Synthesis from First-Principles Calculations. *Science* **2005**, *307*, 555−558.
(18) Cheng, H.; Cui, P.; Wang, F.; Ding, L.; Wang, H. High Efficiency Electrochemical Nitrogen Fixation Achieved with a Lower Pressure Reaction System by Changing the Chemical Equilibrium. *Angew. Chem., Int. Ed.* **2019**, *58*, 15541−15547.
(19) Wang, J.; Yu, L.; Hu, L.; Chen, G.; Xin, H.; Feng, X. Ambient Ammonia Synthesis via Palladium-catalyzed Electrohydrogenation of Dinitrogen at Low Overpotential. *Nat. Commun.* **2018**, *9*, 1795.
(20) Chen, G.; Cao, X.; Wu, S.; Zeng, X.; Ding, L.; Zhu, M.; Wang, H. Ammonia Electrosynthesis with High Selectivity under Ambient Conditions via a Li^+ Incorporation Strategy. *J. Am. Chem. Soc.* **2017**, *139*, 9771−9774.
(21) Nazemi, M.; Panikkanvalappil, S. R.; El-Sayed, M. A. Enhancing the Rate of Electrochemical Nitrogen Reduction Reaction for Ammonia Synthesis under Ambient Conditions using Hollow Gold Nanocages. *Nano Energy* **2018**, *49*, 316−323.
(22) Kozuch, S.; Shaik, S. How to Conceptualize Catalytic Cycles? The Energetic Span Model. *Acc. Chem. Res.* **2011**, *44*, 101−110.
(23) Zhang, L.; Ding, L.-X.; Chen, G.-F.; Yang, X.; Wang, H. Ammonia Synthesis under Ambient Conditions: Selective Electroreduction of Dinitrogen to Ammonia on Black Phosphorus Nanosheets. *Angew. Chem., Int. Ed.* **2019**, *58*, 2612−2616.
(24) Yang, S.; Ye, W.; Zhang, D.; Fang, X.; Yan, D. Layered Double Hydroxide Derived Bimetallic nickel-Iron Selenide as an Active Electrocatalyst for Nitrogen Fixation under Ambient Conditions. *Inorg. Chem. Front.* **2021**, *8*, 1762−1770.
(25) Li, C.; Xu, R.; Ma, S.; Xie, Y.; Qu, K.; Bao, H.; Cai, W.; Yang, Z. Sulfur Vacancies in Ultrathin Cobalt Sulfide Nanoflowers Enable Boosted Electrocatalytic Activity of Nitrogen Reduction Reaction. *Chem. Eng. J.* **2021**, *415*, 129018.
(26) Shinde, S. S.; Sami, A.; Lee, J. H. Electrocatalytic Hydrogen Evolution Using Graphitic Carbon Nitride Coupled with Nanoporous Graphene Co-doped by S and Se. *J. Mater. Chem. A* **2015**, *3*, 12810−12819.
(27) Mushtaq, M. A.; Arif, M.; Fang, X.; Yasin, G.; Ye, W.; Basharat, M.; Zhou, B.; Yang, S.; Ji, S.; Yan, D. Photoelectrochemical Reduction of N_2 to NH_3 Under Ambient Conditions Through Hierarchical $MoSe_2$@g-C_3N_4 Heterojunctions. *J. Mater. Chem. A* **2021**, *9*, 2742−2753.
(28) Arif, M.; Yasin, G.; Luo, L.; Ye, W.; Mushtaq, M. A.; Fang, X.; Xiang, X.; Ji, S.; Yan, D. Hierarchical Hollow Nanotubes of NiFeV-layered Double Hydroxides@CoVP Heterostructures Towards Efficient, pH-universal Electrocatalytical Nitrogen Reduction Reaction to Ammonia. *Appl. Catal., B* **2020**, *265*, 118559−118559.
(29) Chen, P.; Zhang, N.; Wang, S.; Zhou, T.; Tong, Y.; Ao, C.; Yan, W.; Zhang, L.; Chu, W.; Wu, C.; Xie, Y. Interfacial Engineering of Cobalt Sulfide/Graphene Hybrids for Highly Efficient Ammonia Electrosynthesis. *Proc. Natl. Acad. Sci. U. S. A.* **2019**, *116*, 6635−6640.
(30) Ye, W.; Arif, M.; Fang, X.; Mushtaq, M. A.; Chen, X.; Yan, D. Efficient Photoelectrochemical Route for the Ambient Reduction of N_2 to NH_3 Based on Nanojunctions Assembled from MoS_2 Nanosheets and TiO_2. *ACS Appl. Mater. Interfaces* **2019**, *11*, 28809−28817.
(31) Xu, B.; Xia, L.; Zhou, F.; Zhao, R.; Chen, H.; Wang, T.; Zhou, Q.; Liu, Q.; Cui, G.; Xiong, X.; Gong, F.; Sun, X. Enhancing Electrocatalytic N_2 Reduction to NH_3 by CeO_2 Nanorod with Oxygen Vacancies. *ACS Sustainable Chem. Eng.* **2019**, *7*, 2889−2893.
(32) Xie, H.; Geng, Q.; Li, X.; Wang, T.; Luo, Y.; Alshehri, A. A.; Alzahrani, K. A.; Li, B.; Wang, Z.; Mao, J. Ceria-Reduced Graphene Oxide Nanocomposite as an Efficient Electrocatalyst Towards Artificial N_2 Conversion to NH_3 under Ambient Conditions. *Chem. Commun.* **2019**, *55*, 10717−10720.
(33) Zhao, L.; Zhou, J.; Zhang, L.; Sun, X.; Sun, X.; Yan, T.; Ren, X.; Wei, Q. Anchoring Au(111) on a Bismuth Sulfide Nanorod: Boosting the Artificial Electrocatalytic Nitrogen Reduction Reaction under Ambient Conditions. *ACS Appl. Mater. Interfaces* **2020**, *12*, 55838−55843.
(34) Xie, H.; Wang, H.; Geng, Q.; Xing, Z.; Wang, W.; Chen, J.; Ji, L.; Chang, L.; Wang, Z.; Mao, J. Oxygen Vacancies of Cr-Doped CeO_2 Nanorods that Efficiently Enhance the Performance of Electrocatalytic N_2 Fixation to NH_3 under Ambient Conditions. *Inorg. Chem.* **2019**, *58*, 5423−5427.
(35) Zhang, S.; Zhao, C.; Liu, Y.; Li, W.; Wang, J.; Wang, G.; Zhang, Y.; Zhang, H.; Zhao, H. Cu Doping in CeO_2 to form Multiple Oxygen Vacancies for Dramatically Enhanced Ambient N_2 Reduction Performance. *Chem. Commun.* **2019**, *55*, 2952−2955.
(36) Lv, C.; Yan, C.; Chen, G.; Ding, Y.; Sun, J.; Zhou, Y.; Yu, G. An Amorphous Noble-Metal-Free Electrocatalyst that Enables Nitrogen Fixation under Ambient Conditions. *Angew. Chem., Int. Ed.* **2018**, *57*, 6073−6076.
(37) Xiong, H.; Lin, S.; Goetze, J.; Pletcher, P.; Guo, H.; Kovarik, L.; Artyushkova, K.; Weckhuysen, B. M.; Datye, A. K. Thermally Stable and Regenerable Platinum-Tin Clusters for Propane Dehydrogenation Prepared by Atom Trapping on Ceria. *Angew. Chem., Int. Ed.* **2017**, *56*, 8986−8991.
(38) Qi, J.; Gao, L.; Wei, F.; Wan, Q.; Lin, S. Design of a High-Performance Electrocatalyst for N_2 Conversion to NH_3 by Trapping Single Metal Atoms on Stepped CeO_2. *ACS Appl. Mater. Interfaces* **2019**, *11*, 47525−47534.
(39) Tian, J.; Liu, Q.; Asiri, A. M.; Sun, X. Self-Supported Nanoporous Cobalt Phosphide Nanowire Arrays: an Efficient 3D Hydrogen-Evolving Cathode over the Wide Range of pH 0−14. *J. Am. Chem. Soc.* **2014**, *136*, 7587−7590.
(40) Feng, J.; Xu, H.; Dong, Y.; Lu, X.; Tong, Y.; Li, G. Efficient Hydrogen Evolution Electrocatalysis Using Cobalt Nanotubes Decorated with Titanium Dioxide Nanodots. *Angew. Chem., Int. Ed.* **2017**, *56*, 2960−2964.
(41) Watt, G. W.; Chrisp, J. D. Spectrophotometric Method for Determination of Hydrazine. *Anal. Chem.* **1952**, *24*, 2006−2008.
(42) Ye, W.; Yang, Y.; Arif, M.; Yang, S.; Fang, X.; Mushtaq, M. A.; Chen, X.; Yan, D. Fe, Mo-N/C Hollow Porous Nitrogen-Doped

Carbon Nanorods as an Effective Electrocatalyst for N_2 Reduction Reaction. *ACS Sustainable Chem. Eng.* **2020**, *8*, 15946−15952.
(43) Zhao, J.; Liu, X.; Ren, X.; Sun, X.; Tian, D.; Wei, Q.; Wu, D. Defect-Rich ZnS Nanoparticles Supported on Reduced Graphene Oxide for High-Efficiency Ambient N_2-to-NH_3 Conversion. *Appl. Catal., B* **2021**, *284*, 119746.
(44) Xu, X.; Liu, X.; Zhao, J.; Wu, D.; Du, Y.; Yan, T.; Zhang, N.; Ren, X.; Wei, Q. Interface Engineering of MoS_2@$Fe(OH)_3$ Nanoarray Heterostucture: Electrodeposition of MoS_2@$Fe(OH)_3$ as N_2 and H^+ Channels for Artificial NH_3 Synthesis under Mild Conditions. *J. Colloid Interface Sci.* **2022**, *606*, 1374−1380.
(45) Zhao, L.; Liu, X.; Zhang, S.; Zhao, J.; Xu, X.; Du, Y.; Sun, X.; Zhang, N.; Zhang, Y.; Ren, X.; Wei, Q. Rational Design of Bimetallic $Rh_{0.6}Ru_{0.4}$ Nanoalloys for Enhanced Nitrogen Reduction Electrocatalysis under Mild Conditions. *J. Mater. Chem. A* **2021**, *9*, 259−263.

https://doi.org/10.1021/acssuschemeng.1c05850
ACS Sustainable Chem. Eng. 2021, 9, 13399−13405